Journal of Solid State Chemistry 184 (2011) 2936–2940

Contents lists available at SciVerse ScienceDirect

Journal of Solid State Chemistry

journal homepage: www.elsevier.com/locate/jssc

TiO_2 nanorods branched on fast-synthesized large clearance TiO_2 nanotube arrays for dye-sensitized solar cells

Anzheng Hu [a], Haina Li [b], Zhiyong Jia [a], Zhengcai Xia [b,*]

[a] School of Physics and Electronic Engineering, Xiangfan University, Xiangfan 441053, Hubei, PR China
[b] Wuhan National High Magnetic Field Center, Huazhong University of Science and Technology, PR China

ARTICLE INFO

Article history:
Received 19 June 2011
Received in revised form
31 August 2011
Accepted 4 September 2011
Available online 12 September 2011

Keywords:
Branched TiO_2 nanorods
Large clearance nanotubes
Modification
Dye-sensitized solar cells

ABSTRACT

A large clearance TiO_2 nanotube arrays (LTAs) has been synthesized by a not more than 12 h anodization duration and based on this a branched TiO_2 nanotube arrays (BLTs) has been achieved through TiO_2 nanorods branch-like grown on the LTAs. Some key factors and probable mechanisms of the fabrication processes on two novel nanoarchitectures are discussed. Exhilaratingly, it is found that the obtained LTAs has demonstrated large pore diameter and void spaces (pore diameter ~350 nm; void spaces ~160 nm; and tube length ~3.5 μm), and the synthesized hierarchical BLTs, compared with conventional TiO_2 nanotube arrays, has shown a much stronger dye absorption performance and an approximately double of the solar cell efficiency (in our case from 1.62% to 3.18% under simulated AM 1.5 conditions).

1. Introduction

There is no doubt about the significance of dye-sensitized solar cells (DSCs, also known as Grätzel cells) with the cost-effective and relatively high photoconversion efficiency for a new renewable and clean energy development and utilization, and there is either doubt about the necessity of finding optimum electrode materials [1–10]. As one excellent semiconductor with non-toxic and wide band gap (3.2 eV for anatase, 3.0 eV for rutile) [11], TiO_2 has attracted considerable interest for its promising applications such as DSCs [5–7,12–14], photocatalysts [15–17], photoelectronchemical cells [18], sensors [19], electrochromic devices [20], and so on. In recent years, more and more researchers have devoted themselves to the synthesis of one-dimensional (1D) nanostructure TiO_2 with different morphological structures [21] such as nanotubes [3,5–7,13,14,22], nanorods [23,24], and nanowires [25,26], in order to facilitate electron transport through the suppression of random walk phenomena from these structures. The tubular structure and tunable pore size of TiO_2 nanotube arrays (TNAs) have attracted special attention [12–20] including the impressive progress made in tuning the length, wall thickness, diameter, and building pattern order of TNAs, and the conversion efficiencies in DSCs have steadily been improved up to approximately 3% (AM 1.5 light illumination) with better electrode structures [12,27–30]. At present, some attention has been paid to re-modification of TNAs. For example, Au-coated, carbon-doped and TiO_2 nanoparticles-decorated TNAs have been synthesized [31–33,6] for better performance in solar water splitting, DSCs, and organic pollutants detection; the CNT@TiO_2 core/porous-sheath coaxial nanocables were also synthesized and used as anode materials for lithium-ion batteries [34]. However, to the best of our knowledge, no attention has been yet focused on the investigation of branched TiO_2 nanotube arrays (BLTs) based on the large clearance TiO_2 nanotube arrays (LTAs) for DSCs.

In this work, we report on the fabrication of BLTs via two-step route of electrochemical anodization and hydrothermal modification. Specifically, the first step is the synthesis of LTAs by anodization of Ti foils in an electrolyte containing lactic acid, NH_4F and DMSO. The obtained LTAs have a large average pore diameter of ~350 nm, big void spaces among tubes of ~160 nm, and longer length of ~3.5 μm, and in the synthesis process it is formated under a very short anodization durations of about 12 h, which is just 10% of approximately 120 h reported in the previous references [35,36]. More interestingly, the large void spaces facilitate intercalation of the decorating and loading materials into the nanotubes, thus improving interfacial contact between the TiO_2 and the loading materials including sensitizing dyes for superior exciton dissociation.

The second step is the synthesis of BLTs by hydrothermal approach. In particular, the key factors and the probable mechanisms on synthesis process of BLTs are also investigated. Furthermore, using as-synthesized LTAs, BLTs and conventional TNAs as photoanodes, their light absorption and conversion efficiencies in

* Corresponding author. Fax: +86 710 3591876.
E-mail addresses: sporthaz@126.com (A. Hu), xia9020@public.wh.hb.cn (Z. Xia).

0022-4596/$ - see front matter © 2011 Elsevier Inc. All rights reserved.
doi:10.1016/j.jssc.2011.09.005

DSCs are tested and compared. Result shows that photoconversion efficiencies of the LTAs and BLTs are greatly improved from 1.62% of TNAs to 1.87% and 3.18%, respectively. As a result, it would be reasonable to believe that the LTAs and BLTs with such large pore size will become the promising candidates for applications in sensors, photocatalysis, and drug delivery.

2. Experimental details

2.1. Synthesis of LTAs

In this paper, the LTAs was obtained through a typical anodization approach, in which a two-electrode anodization setup was made by ourselves with Ti foil as the anode and Pt foil as the cathode (see Fig. 1a and b). At first, a 0.25 mm thick Ti foil sample (Purity $\geq$ 99.7%, Sigma Aldrich, about 2 cm $\times$ 3.5 cm per foil), was burnished with metallographic sand paper, immersed in the chemical polishing solution with $HF:HNO_3:H_2O=1:1:2$ (volume ratio) to remove oxide layer and blot. At the same time, the sample was cleaned with soap, acetone, and isopropanol before and after chemical polishing. And then, the prepared Ti foil sample was immersed in the electrolyte of lactic acid (purity 85.0%) and 10 vol% DMSO (dimethyl sulphoxide: purity $\geq$ 99.0%) containing 0.35 wt% NH_4F firstly under the applied voltages of 55 V for approximately 15 min, and then at 50 V for 12 h. Temperature of electrolyte was controlled at approximately 35 °C through the whole anodization. After anodization, the as-prepared amorphous LTAs were rinsed with isopropyl alcohol, soaked, and ultrasonicated with acetone and alcohol, and then dried in air. Subsequently, the LTAs were annealed at 400 °C for 1 h and then cooled at rate of 30 °C/min to achieve anatase structures [37] for further use.

2.2. Formation of BLTs

The new hierarchical BLTs were achieved by growing TiO_2 nanorods on the as-prepared LTAs through a conventional hydrothermal growth approach. The prepared LTAs were immersed in a beaker with named as growth solution. This solution was prepared with aqueous solutions of 0.6 M HCl (36–38%) with constant stirring at room temperature for about 15 min. Subsequently, TTIP of 8 vol% was dropped (at rate 0.16 μL/s) in a mixture solution, and kept stirring for more than 1 h [5]. And then the beaker was sealed and placed into constant temperature water-bath setup, maintained at 95 °C for 7–12 h to grow TiO_2 nanorods on the LTAs. The BLTs were finally achieved after the reactants were cooled freely, washed with ethanol and distilled water, and heated at 400 °C for 2 h [32] (see Fig. 1).

2.3. Characterization and DSCs properties testing

The samples' morphologies (pore size, tubes clearance, and length) were observed by field-emission scanning electron microscopy (FESEM, JOEL, JSM-6700F), and transmission electron microscopy (TEM, JEM-2010FEF; 200 kV). And their crystal phase structures were characterized with a Bruker D8 advance X-ray diffractometer (XRD, Cu $K\alpha$; 1.5418 Å). DSCs were used to characterize photoelectrochemical properties of three new electrodes of LTAs, BLTs, and TNAs. To obtain information on dye loading, dye desorption experiments were carried out by immersing the samples in an alcohol solution of 0.5 mM N719 (Ruthenium 535 bis-TBA, Dyesol, Australia) for 24 h followed by photometric dye concentration measurements [27]. After dye-sensitization, the samples were rinsed with ethanol to remove the excess nonchemisorbed dye. And then, the dye-adsorbed electrodes with an active area of 0.2 cm^2 were assembled into the sandwich-type cell, with FTO glass deposited Pt by a sputtering method as a counter electrode. The inner space was filled up with a liquid electrolyte consisting of 0.5 M LiI, 0.05 M I_2, and 0.5 M tert-butyl pyridine in methoxypropionitrile as a redox arbiter. Photocurrent–voltage characteristics of the cells were measured under simulated AM 1.5 illumination provided by solar simulator (1 kW Xe with optical filter, Oriel) with an intensity of 100 mW/cm^2 [27,38].

3. Results and discussion

3.1. Schematic of synthesis BLTs

The schematic diagram of fabrication BLTs by two-step method is shown in Fig. 1. The electrochemical setup of anodization designed by ourselves is presented in Fig. 1a. The schematic diagram (Fig. 1a and b) is used to present lots of visual information of synthesis LTAs, such as fabrication process, composition of electrolyte, applied voltage, anodization duration, and so on. Analogously, the information about growing TiO_2 nanorods on LTAs by the hydrothermal decoration approach is shown in Fig. 1b and c. Furthermore, it is discovered in our experiment that one of the necessary conditions to achieve BLTs of good quality is that the TiO_2 nanotube arrays framework must possess larger pore size, more void spaces among tubes (named as large clearance), and rougher surface area. Considering that these nanorods are directly grown on the nanotubes, the as-prepared hierarchical BLTs will provide both the more facilitated entrance for TiO_2 crystal nucleus and the rougher surface area to be in favour of implanting of nucleus and then freely growing up and becoming into anisotropic 1D TiO_2 nanorods along the backbones of the LTAs [32].

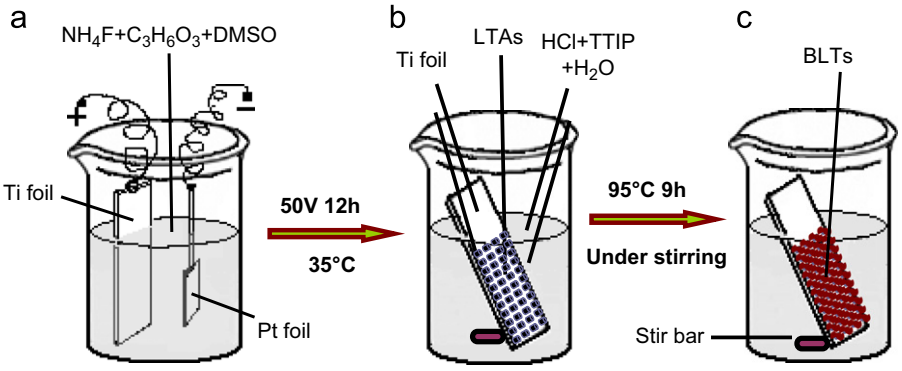

Fig. 1. Schematic of synthesis BLTs via two-step method of electrochemical anodization and hydrothermal modification.

3.2. Fabrication investigation of LTAs

To obtain optimal nanoarchitecture LTAs, many influencing factors, such as electrolyte composition, anodization duration, applied voltage, temperature of electrolyte, chemical polishing process of Ti foil, ultrasonic treatment of amorphous nanotubes, and so on, were systematically investigated. Two key factors deserve special discussion here: one is the concentration of added DMSO in $NH_4F/C_3H_6O_3$ electrolyte, and the other is the applied voltage, as-shown in Fig. 2. With anodization time of 12 h and DMSO concentration of 10 vol%, the performances of the voltage-dependent pore sizes are shown in Fig. 2a. It is no surprise that the pore diameter increases as anodization potential [35,36], but it is also discovered that the morphologies and structures of formed tubes can be destroyed (see the SEM images in Fig. 3f) with voltage of more than 60 V and anodization time of more than 12 h. Otherwise, the nanotube arrays with 380 nm pore diameter were achieved under 60 V for about 8 h (Fig. 3g), but the length of nanotube is not more than 1.5 μm, which is not expected because stronger internal light-scattering effects and enhanced charge-collection efficiencies come from longer TiO_2 nanotuble arrays [39]. In our electrolyte system, 50 V is the optimum applied voltage, and the largest pore diameter is about 350 nm. As for another key factor, Fig. 2b is employed to present the result of the variation of tube length as a function of anodization time under different concentrations of DMSO: 7 vol%, 10 vol%, and 14 vol%. From the function curves, we can clearly observe that the largest length of tube is 3.5 μm coming from the DMSO content 10 vol% and anodization time of 12 h. Through the processes of 50 V for 12 h after 55 V anodization 15 min, we can obtain optimized LTAs. The cause may be easily conceived that foregoing applied voltage of 55 V for 15 min is used to form the larger pore core at the beginning. Otherwise, it is worth noticing that there are few reports concerning the synthesis of large pore diameter TiO_2 nanotube arrays by anodizing methods in past two years [35,36]. But, in those reports, the anodization duration is more than 120 h, which is ten times of 12 h (in our anodization approach).

3.3. Morphologies and microstructures of LTAs and BLTs

Fig. 3(a–e) presents characterization images of the optimized nanoarchitecture LTAs. Specifically, Fig. 3a is the top view SEM image of low-magnification, with the inset as its significantly enlarged image; Fig. 3b and c shows images of high-magnification and a cross-section, respectively; Fig. 3d is TEM image of individual tube with the insets as its HRTEM and SAED images of the marked areas; and Fig. 3e is a optical image of as-obtained LTAs; Fig. 3f and g shows images of the excessive voltage and oxide etching, respectively. From Fig. 3a–c and 3e, it can be clearly found that the LTAs not only show very good morphologies characterization (self-organized, high-ordered, free-standing, etc.), but show the optimized geometrical architectures and the large clearance: large external pore diameter ~350 nm; long tube length ~3.5 μm; big void spaces ~160 nm; and very rough surface structure. Furthermore, we can find in Fig. 3d that the obtained LTAs show at least local single-crystalline structure (see inset of the SAED in Fig. 3d), the (101) crystal facet and the 0.35 nm interplane distance of a typical anatase TiO_2 [21,39] (see inset HRTEM in Fig. 3d).

Fig. 4 shows us the very nice images on the morphologies and microstructures characterization of BLTs (see Section 2.2). Specifically, Fig. 4a and 4b present the top view SEM images of low-magnification and significantly enlarged BLTs; Fig. 4c and d are its cross-section images; Fig. 4e is TEM image of individual BLTs, with the inset in Fig. 4e and f as its SAED and HRTEM images in the marked areas, respectively. By observing the morphologies of the top view, cross-section, especially enlarged images, we can find that numerous TiO_2 nanorods (with very proper length, density, and diameter) branch along the entire surface of LTAs skeleton. Considering that the nanorods are directly aligned on the surface of nanotubes array LTAs to form hierarchical arrays that will provide both large active surface areas for dye absorption and good electron transport for fast redox kinetics, which is just expected to boost higher solar cell efficiency. Furthermore, by

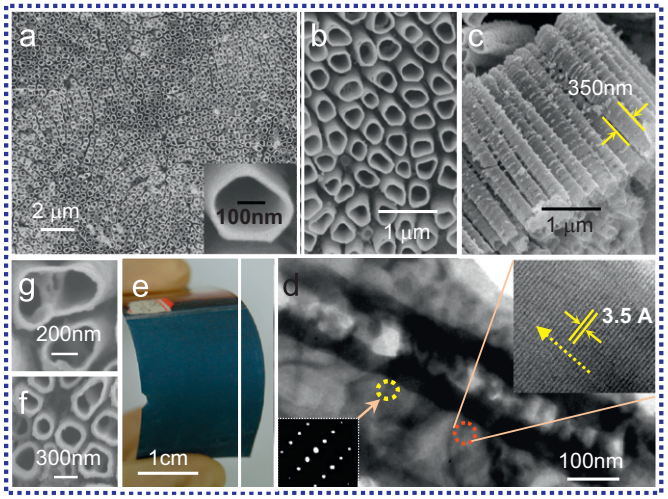

Fig. 3. Characterization images of the LTAs: (a) Low-magnification (insets are enlarged), (b) high-magnification, (c) cross-section SEM images, (d) TEM image of individual LTAs, insets are its HRTEM and SAED images of the marked areas, respectively, (e) optical images, and (f,g) general SEM images.

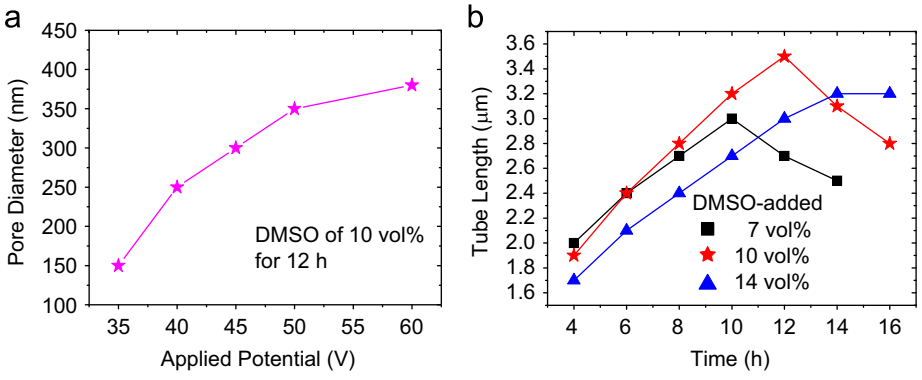

Fig. 2. (a) Pore sizes of TiO_2 nanotubes as a function of voltage and (b) lengths of nanotubes as a function of anodization duration of different DMSO-containing in electrolyte, voltage is 50 V.

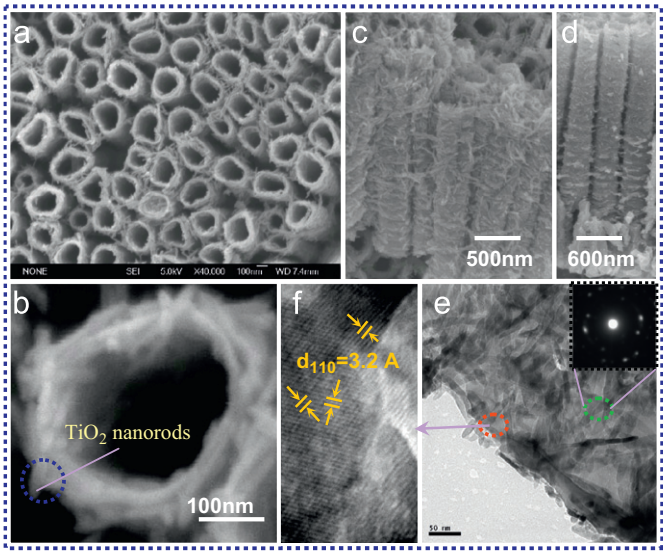

Fig. 4. (a) Low-, (b) high-magnification, (c,d) cross-section SEM images of BLTs, (e) TEM image of individual BLTs, inset and (f) are its SAED and HRTEM images in the marked areas, respectively.

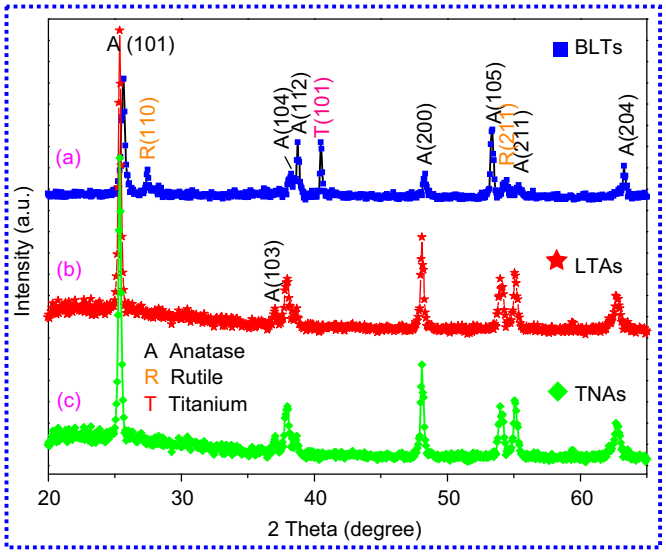

Fig. 5. XRD patterns of three as-obtained samples: (a) BLTs, (b) LTAs, and (c) TNAs.

analyzing the SAED and HRTEM images, result shows that BLTs is the polycrystalline structure composed of the anatase-dominated LTAs skeleton and the branched TiO_2 nanorods, which is rutile phase with (110) crystal facet and the 0.32 nm interplane distance of a typical rutile TiO_2 [5].

3.4. XRD analysis

The XRD patterns (Fig. 5a–c) are employed to characterize the properties of three obtained arrays: BLTs, LTAs, and TNAs. With comparison, it can be found that the dominant diffraction peaks of three samples (a–c) are identified as the (101) peak at 2θ 25.3°. Especially, the XRD patterns in Fig. 5b and c match very well with the crystal structure of the anatase phase TiO_2 (see JCPDS Card No. 21-1272) [40] except for one peak of the Ti (101). The results attribute to thermal treatment process of not more than 400 °C for 2 h. Otherwise, it is noteworthy that the two peaks [R (110) and R (211)] of BLTs in Fig. 5a just match with the crystal structure of the rutile TiO_2 (JCPDS Card No. 21-1276) [5,30], and

Table 1
Photovoltaic performance parameters of DSCs under simulated AM 1.5 solar light illumination.

Photoanodes	J_{sc} (mA/cm^2)	V_{oc} (V)	FF	η (%)	Dye loading (mM)
BLTs	6.48	0.76	0.58	3.18	88
LTAs	3.86	0.73	0.60	1.87	66
TNAs	3.72	0.72	0.54	1.62	58

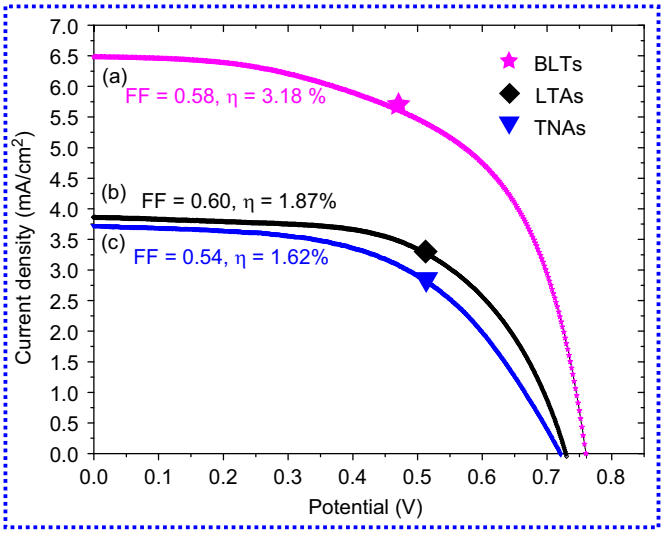

Fig. 6. *I–V* characteristics of DSCs for three different photoanodes: (a) BLTs, (b) LTAs, and (c) TNAs) under simulated solar light illumination.

it is not difficult to be imagined with those rutile phase TiO_2 nanorods grown on the TNAs. The conclusions are accordance with those from SAED patterns and HRTEM images (Fig. 4e and f).

3.5. Photovoltaic characteristics of DSCs

Three as-synthesized samples (BLTs, LTAs, and TNAs) were annealed and dye-sensitized under the same conditions. For a detailed evaluation of their solar cells properties, their *I–V* characteristics of DSCs were measured under simulated AM 1.5 solar light illumination. By comparison, many photovoltaic performance parameters (FF, dye loading, *I–V* characteristics) are summarized in Table 1 and Fig. 6. We can evidently find that, from Table 1 and Fig. 6, the BLTs presents the highest solar cell efficiency of 3.18%, which is approximately doubling of 1.62% from TNAs in our case. Quite interestingly, the FF values of BLTs and LTAs are both higher than that of TNAs and their *I–V* curves show much better rectangle shapes accordingly (see Fig. 6a–c). One of the causes may be associated with the different dye loading from three electrodes [6]. By observing Table 1, it can also be found that the dye loading of the sample BLTs is significantly higher than that of sample TNAs (88–58 mM). We can imagine that the tremendousness of dye absorption of sample BLTs results from the significantly increased surface areas provided by the huge amounts of TiO_2 nanorods. Otherwise, the relatively higher values of dye loading (66–58 mM), conversion efficiency (1.87–1.62%) and better FF values (60–54) of sample LTAs can be attributed to its larger pore diameter and void spaces than that of sample TNAs.

4. Conclusions

We have achieved an electrode material (BLTs) with higher dye absorption performance and significantly solar cell efficiency,

and the BLTs is synthesized by TiO_2 nanorods branch-like grown on fast-synthesized large pore diameters and void spaces TiO_2 nanotube arrays (LTAs). Interestingly, the as-synthesized BLTs and LTAs with beautiful morphologies and large clearance show both larger and rougher surface areas. Moreover, the improvement of about double of the photoconversion efficiencies from 1.62% of TNAs to 3.18% of BLTs is also achieved. As a result, we believe that the LTAs and BLTs with such large void spaces will become the promising candidates for applications in sensors, photocatalysis, drug delivery, and so on.

Acknowledgments

The authors would like to acknowledge the financial support for this study from the Xiangyang Plans Projects of Scientific and Technological Research and Development (No. 2010GG1B35).

References

[1] P. Poizot, S. Laruelle, S. Grugeon, L. Dupont, J.M. Tarascon, Nature 407 (2000) 496–499.
[2] M. Armand, J.M. Tarascon, Nature 451 (2008) 652–657.
[3] G.K. Mor, K. Shankar, M. Paulose, O.K. Varghese, C.A. Grimes, Nano Lett. 6 (2006) 215–218.
[4] A.S. Arico, P. Bruce, B. Scrosati, J.M. Tarascon, W. Van Schalkwijk, Nat. Mater. 4 (2005) 366–377.
[5] Y.S. Oh, J.K. Lee, H.S. Kim, S.B. Han, K.W. Park, Chem. Mater. 22 (2010) 1114–1118.
[6] P. Roy, D. Kim, I. Paramasivam, P. Schmuki, Electrochem. Commun. 11 (2009) 1001–1004.
[7] J. Wang, Z.J. Lin, Chem. Mater. 20 (2008) 1257–1261.
[8] S.Y. Chung, J.T. Bloking, Y.M. Chiang, Nat. Mater. 1 (2002) 123–128.
[9] K.S. Kang, Y.S. Meng, J. Breger, C.P. Grey, G. Ceder, Science 311 (2006) 977–980.
[10] B. Kang, G. Ceder, Nature 458 (2009) 190–193.
[11] A. Bendavid, P.J. Martin, A. Jamting, H. Takikawa, Thin Solid Films 355 (1999) 6–11.
[12] D. Kim, A. Ghicov, S.P. Albu, P. Schmuki, J. Am. Chem. Soc. 130 (2008) 16454–16455.
[13] D.A. Wang, Y. Liu, C.W. Wang, F. Zhou, W.M. Liu, ACS Nano 3 (2009) 1249–1257.
[14] U. Bach, D. Lupo, P. Comte, J.E. Moser, F. Weissortel, J. Salbeck, H. Spreitzer, M. Gratzel, Nature 395 (1998) 583–585.
[15] N. Negishi, T. Iyoda, K. Hashimoto, A. Fujishima, Chem. Lett. 9 (1995) 841–842.
[16] D.A. Wang, T.C. Hu, L.T. Hu, B. Yu, Y.Q. Xia, F. Zhou, W.M. Liu, Adv. Funct. Mater. 19 (2009) 1930–1938.
[17] S. Meng, J. Ren, E. Kaxiras, Nano Lett. 8 (2008) 3266–3272.
[18] K. Shin, S.I. Seok, S.H. Im, J.H. Park, Chem. Commun. 46 (2010) 2385–2387.
[19] Q. Zheng, Q. Zhou, J. Bai, L.H. Li, Z.J. Jin, J.L. Zhang, J.H. Li, Y.B. Liu, W.M. Cai, X.Y. Zhu, Adv. Mater. 20 (2008) 1044–1049.
[20] R. Cinnsealach, G. Boschloo, S.N. Rao, D. Fitzmaurice, Sol. Energy Mater. Sol. Cell. 55 (1998) 215–223.
[21] X.B. Chen, S.S. Mao, Chem. Rev. 107 (2007) 2891–2959.
[22] M. Paulose, K. Shankar, O.K. Varghese, G.K. Mor, B. Hardin, C.A. Grimes, Nanotechnology 17 (2006) 1446–1448.
[23] H. Xu, F. Jia, Z. Ai, L. Zhang, Cryst. Growth Des. 7 (2007) 1216–1219.
[24] M.Y. Song, D.K. Kim, K.J. Ihn, S.M. Jo, D.Y. Kim, Nanotechnology 15 (2004) 1861–1865.
[25] Q. Shen, T. Sato, M. Hashimoto, C. Chen, T. Toyoda, Thin Solid Films 499 (2006) 299–305.
[26] L. Francioso, A.M. Taurino, A. Forleo, P. Siciliano, Sen. Actuators B Chem. 130 (2008) 70–76.
[27] D. Kim, A. Ghicov, P. Schmuki, Electrochem. Commun. 10 (2008) 1835–1838.
[28] S.P. Albu, A. Ghicov, S. Aldabergenova, P. Drechsel, D. LeClere, G.E. Thompson, J.M. Macak, P. Schmuki, Adv. Mater. 20 (2008) 4135–4139.
[29] G.K. Mor, K. Shankar, M. Paulose, O.K. Varghese, C.A. Grimes, Nano Lett. 5 (2005) 191–195.
[30] L. Liu, J.S. Qian, B. Li, B. Cui, X.F. Zhou, X.F. Guo, W.P. Ding, Chem. Commun. 46 (2010) 2402–2404.
[31] J.H. Park, S. Kim, A.J. Bard, Nano Lett. 6 (1) (2006) 24–28.
[32] A.Z. Hu, C.X. Cheng, X. Li, J. Jiang, R.M. Ding, X.T. Huang, et al., Nano. Res. Lett. 6 (2011) 91.
[33] X.H. Li, G.Y. Chen, L.B. Yang, Z. Jin, J.H. Liu, Adv. Funct. Mater. 20 (2010) 2815–2824.
[34] F.F. Cao, Y.G. Guo, S.F. Zheng, X.L. Wu, et al., Chem. Mater. 22 (2010) 1908–1914.
[35] S. Yoriya, C.A. Grimes, Langmuir 26 (1) (2010) 417–420.
[36] A. Mohammadpour, P.R. Waghmare, S.K. Mitra, K. Shankar, ACS Nano 4 (12) (2010) 7421–7430.
[37] R. Beranek, H. Tsuchiya, T. Sugishima, J.M. Macak, L. Taveira, S. Fujimoto, H. Kisch, P. Schmuki, Appl. Phys. Lett. 87 (2005) 243114–243116.
[38] A. Ghicov, S. Albu, R. Hahn, D. Kim, T. Stergiopoulos, J. Kunze, C.-A. Schiller, P. Falaras, P. Schmuki, Chem. Asian J. 4 (2009) 520–525.
[39] K. Zhu, N.R. Neale, A. Miedaner, A.J. Frank, Nano Lett. 7 (2007) 69–74.
[40] X.F. Xiao, K. Ouyang, R.F. Liu, J.H. Liang, Appl. Surf. Sci. 255 (2009) 3659–3663.